

We are IntechOpen, the world's leading publisher of Open Access books Built by scientists, for scientists

6,900

Open access books available

186,000

International authors and editors

200M

Downloads

Our authors are among the

154

Countries delivered to

TOP 1%

most cited scientists

12.2%

Contributors from top 500 universities



WEB OF SCIENCE™

Selection of our books indexed in the Book Citation Index
in Web of Science™ Core Collection (BKCI)

Interested in publishing with us?
Contact book.department@intechopen.com

Numbers displayed above are based on latest data collected.
For more information visit www.intechopen.com



Synchrotron Radiation Microangiography for Investigation of Metabolic Syndrome in Rat Model

Keiji Umetani¹, Kazuhito Fukushima² and Kazuro Sugimura³

¹*Research & Utilization Division, Japan Synchrotron Radiation Research Institute*

²*Research Institute, National Cardiovascular Center*

³*Department of Radiology, Kobe University School of Medicine
Japan*

1. Introduction

Imaging research for preclinical in-vivo small animal studies has pursued development of high spatial resolution scanners to reveal fine details in rats, mice, and rabbits since the mid-1990s because drugs can be tested more easily in animals than in humans (Service, 1999; Ritman, 2002). Laboratory animal imaging plays a decisive role in drug discovery and in elucidating the mechanisms of disease. In terms of basic laboratory investigations using CT, positron emission tomography, magnetic resonance imaging, optical imaging, and ultrasound, preclinical laboratory animal imaging modalities are becoming valuable research tools for investigating biology and disease (Colby & Morenko, 2004).

Medical imaging using synchrotron radiation has been utilized as a safe intravenous angiography technique since the end of the 1970s. This safe intravenous angiography technique is useful in place of conventional selective coronary arteriography. Research groups in several synchrotron radiation facilities have improved imaging systems for human studies (Rubenstein et al., 1986; Dix et al., 2003). In addition to intravenous coronary angiography, an intra-arterial high-resolution angiography system with spatial resolution of 20 μm was developed at the Photon Factory (Tsukuba, Japan) for use in laboratory animal studies (Mori et al., 1996).

Subsequently, a new microangiography system with spatial resolution as high as 10 μm was developed at SPring-8 using an X-ray direct-conversion type detector incorporating an X-ray SATICON pickup tube. The imaging system has been used at the BL20B2 beamline for depiction of tumor-derived angiogenic vessels in a rabbit model of cancer (Umetani et al., 2003) and microvascular reactivity in transgenic mice (Yamashita et al., 2002). The beamline instrumentation, incorporating X-ray optical and imaging devices, provides synchrotron radiation users with a high-flux monochromatic X-ray beam for imaging experiments. The imaging system has been improved with respect to spatial resolution and exposure time (shutter speed) at another beamline, the BL28B2 beamline, to obtain sequential, sharp, blur-free images of hearts (Iwasaki et al., 2007; Umetani et al., 2008) and brains (Kidoguchi et al., 2006; Morishita et al., 2006) in rats and mice.

For conventional microangiography, an X-ray generator with a small focal spot has been employed using an X-ray direct-conversion type VIDICON camera as a two-dimensional high-resolution detector (Sada et al., 1985; Shirai et al., 1999). However, the X-ray generator system has limited capability for displaying *in vivo* images of blood vessels smaller than 50- μm diameter because images cannot be magnified without blurring as a result of its focal-spot dimensions. The only X-ray source is a synchrotron that can produce small blood vessel images with diameters of less than 50 μm .

Metabolic syndrome refers to a clustering of cardiovascular disease risk factors including obesity, insulin resistance, unhealthy lipid levels, and hypertension (Grundy et al., 2004). Patients exhibiting this syndrome are known to be at higher risk of cardiovascular disease, and insulin resistance confers increased risk for type 2 diabetes mellitus. Hypertension and diabetes can cause damage to the inner walls of arteries. We investigated the characteristics of vascular endothelial function in coronary arteries of rats using a microangiography technique for visualizing vascular diameter changes produced by vasoactive agents. Synchrotron radiation imaging can generate high-resolution and high-speed images with spatial resolution in the micrometer range. For this study of a rat heart under Langendorff perfusion, coronary microangiography was performed with spatial resolution of 6 μm and exposure time of 2 ms. Using rat models of hypertension and diabetes, we performed radiographical evaluation of changes in small coronary arteries by clearly depicting vasodilatation of coronary arteries under the influence of vasoactive agents: acetylcholine, adenosine triphosphate, and sodium nitroprusside (Umetani et al., 2004).

2. Imaging system

Experimental arrangements at the BL28B2 beamline for biomedical imaging using monochromatic synchrotron radiation X-rays are presented in Fig. 1. Coronary and cerebral microangiographic imaging was conducted at the BL28B2 (Kidoguchi et al., 2006; Morishita et al., 2006; Iwasaki et al., 2007; Umetani et al., 2008) because this beamline, which uses a single $\langle 111 \rangle$ silicon crystal monochromator, produces higher flux X-rays than those at the BL20B2, which uses a double $\langle 311 \rangle$ crystal monochromator.

A useful source of synchrotron radiation is a storage ring, which uses bending magnets to maintain an electron beam at relativistic speeds in a closed trajectory for many hours. By bending the path of electrons at relativistic speeds, X-rays are emitted at each bending magnet in a direction that is tangential to the beam trajectory, as portrayed in Fig. 1. Synchrotron radiation generated by bending magnets produces a fan-shaped beam and has a broad and continuous spectrum from infrared to the X-ray region. The single crystal monochromator selects a single energy of synchrotron radiation. Consequently, X-rays with a small energy bandwidth are used for imaging. The monochromatic X-ray energy was adjusted by the monochromator to 33.2 keV just above the iodine K-edge energy to produce the highest contrast image of the iodine contrast agent.

An X-ray imaging system must have a high shutter speed (short exposure time) to produce sharp and blur-free images of objects. For high-speed imaging, we developed an X-ray shutter system using a moving-coil galvanometer-based optical scanner to produce pulsed monochromatic X-rays. The shutter is situated between the monochromator and the object in Fig. 1. An optical scanner is a high-accuracy mirror-positioning motor for laser optics. Figure 2 shows that after an optical mirror was removed from the galvanometer-based

scanner, a rotating X-ray chopper was attached to the center shaft of the scanner. Twin tantalum blades on each side of the chopper move in a seesaw-like manner, synchronizing timing with the synchronous signals of the video camera. By about 9° rotation of the chopper, the shutter opens or closes a route for the X-ray beam. The exposure time per image was finally adjusted to 2–4 ms using the shutter (Umetani et al., 2004).

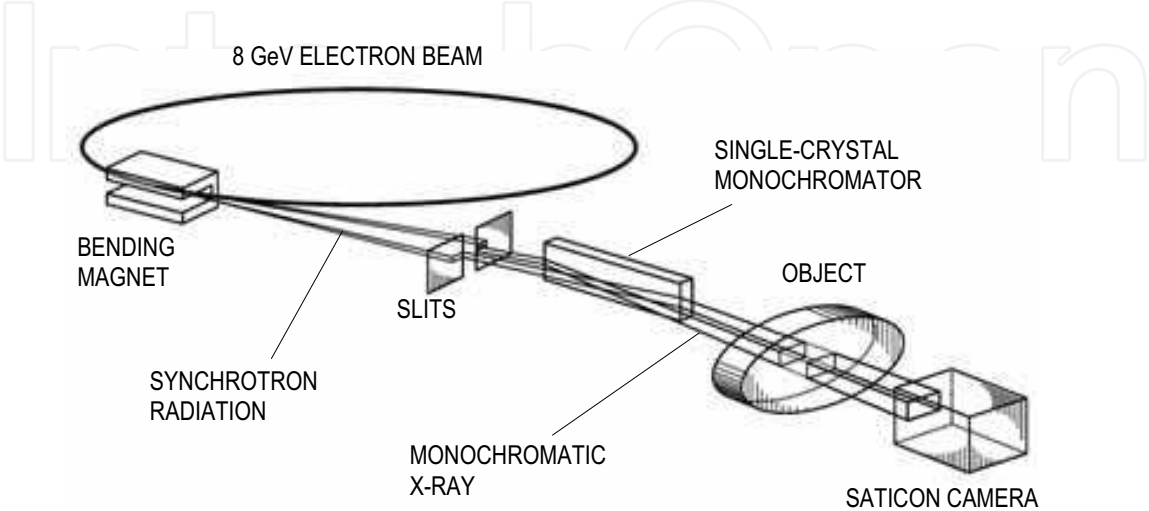


Fig. 1. Experimental arrangement for synchrotron radiation microangiographic imaging.

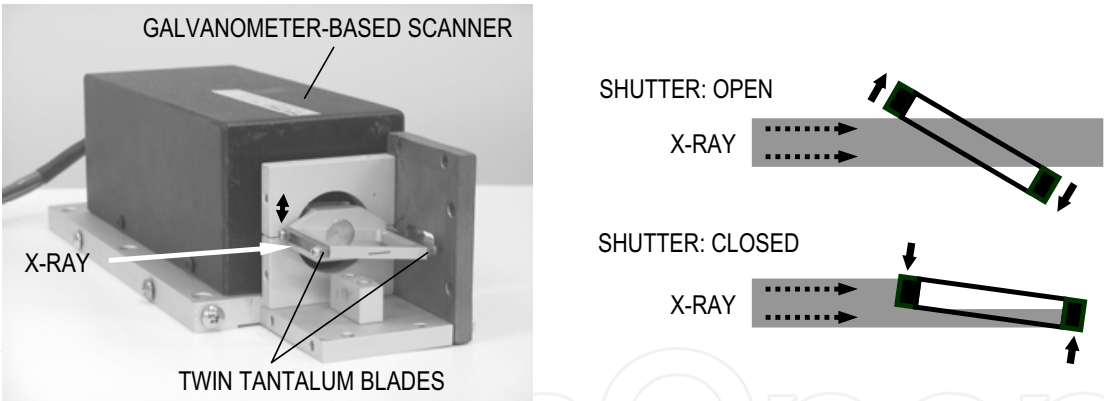


Fig. 2. Photograph of the X-ray shutter (left) and illustration of the chopper action (right).

Pulsed monochromatic X-rays transmitted through the object are detected using the X-ray direct-conversion type detector depicted in Fig. 3, which incorporates the X-ray SATICON pickup tube. The camera system comprises a camera head incorporating the X-ray SATICON pickup tube and a camera control unit with an analog-to-digital converter for digital signal output. The X-ray direct-conversion type SATICON tube consists of a photoconductive target layer of amorphous selenium. Absorbed X-rays in the photoconductive layer of the tube are converted directly into electron-hole pairs. Charge carriers generated by X-rays are transported across the photoconductive layer by an electric field. Then, a charge-density pattern is formed on the photoconductive layer surface. To

produce a video signal, a scanning beam of low-velocity electrons reads out the electrostatic image on the surface.

This X-ray SATICON camera for biomedical imaging has resolution of 1050 scanning lines. It can record images at a maximum rate of 30 frame/s. Sequential images were obtained with an input field of view of $4.5 \text{ mm} \times 4.5 \text{ mm}$. By synchronizing the timing with the camera's synchronous pulse signals, image signals can be converted into a digital format and stored in a frame memory with a format of 1024×1024 pixels and 10-bit resolution. An equivalent pixel size projected onto the input window was $4.5 \text{ }\mu\text{m}$ for a 1024×1024 -pixel format.

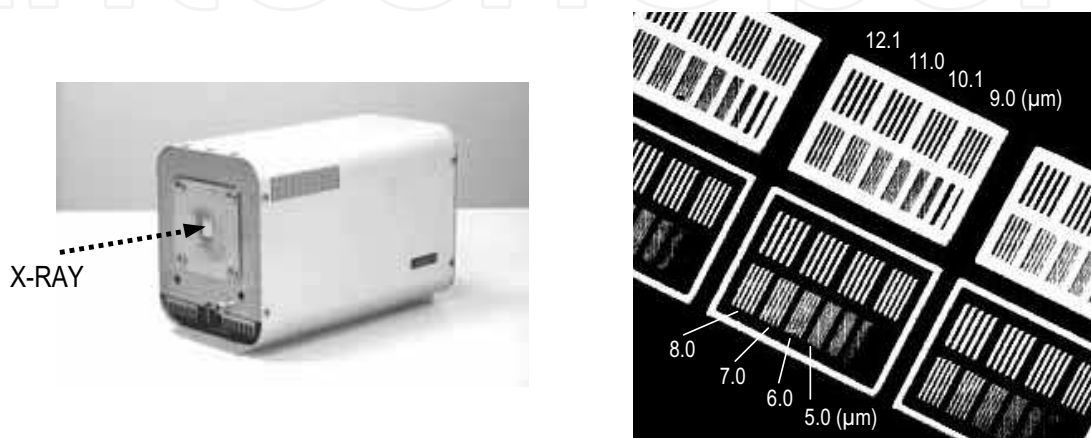


Fig. 3. Photograph of the X-ray SATICON camera (left) and zoomed image of the central area of the 5- μm -thick chart. Numerical values show bar widths (right).

The input field of view of the X-ray SATICON camera was adjusted to $9.5 \text{ mm} \times 9.5 \text{ mm}$ for depiction of tumor-derived angiogenic vessels in a rabbit model of cancer (Umetani et al., 2003). In coronary microangiography, the detector's input field of view was reduced to $4.5 \text{ mm} \times 4.5 \text{ mm}$ for higher spatial resolution imaging. Performance of the direct-conversion type detector was evaluated by taking images of a custom-designed gold resolution chart. The chart thickness was $5 \text{ }\mu\text{m}$; the bar pattern widths were 5.0 – $12.1 \text{ }\mu\text{m}$. An X-ray image of the chart with micrometer-scale bar patterns was obtained in the zoom-imaging mode of the detector with the $4.5 \text{ mm} \times 4.5 \text{ mm}$ field of view at an X-ray energy of 20.0 keV . Figure 3 (right) presents an image of the 5- μm -thick chart in which the $6.0\text{-}\mu\text{m}$ -wide bars are visible. The limiting spatial resolution is between 5.0 and $6.0 \text{ }\mu\text{m}$ in the zoom imaging mode. The $6.0 \text{ }\mu\text{m}$ bar width is comparable to the capillary blood vessels' size. Images of the capillaries are obtainable using an X-ray energy of 33.2 keV just above the iodine K-edge energy, which produces the highest contrast image of the iodine contrast agent if capillaries are opacified using a high-density contrast agent. In reality, however, the contrast agent is diluted substantially in the blood flow.

The distance between the source in the bending magnet and the detector is about 46 m . A nearly parallel X-ray beam was used for imaging without image blur because of the small X-ray source and the extremely long source-to-object distance. The storage ring was operated at 8 GeV electron beam energy; the beam current was 100 mA . Monochromatic X-ray energy

was adjusted to 33.2 keV using the monochromator. The X-ray flux at the object position was ca. 1×10^{10} photon/mm²/s in imaging experiments.

3. Angiographic Imaging

3.1 Animal experiments

Acetylcholine, adenosine triphosphate, and sodium nitroprusside are vasoactive agents inducing endothelium-dependent vasodilatation through the release of endogenous nitric oxide, a nitro vasodilator. We conducted an experimental study of microangiography in isolated perfused rat hearts to evaluate the vascular response for vasoactive agents by measuring internal diameters of small blood vessels on the baseline and under stress of vasoactive agents in rat models of hypertension and diabetes.

Wistar rats weighing about 300 g were used for imaging. The rats were anesthetized with sodium pentobarbital, after which heparin, an anticoagulant, was administered intraperitoneally. After an abdominal incision was made, the heart was excised. The isolated rat heart was mounted on a steel cannula, secured with a suture, as portrayed in Fig. 4, and perfused with oxygenated perfusion fluid (a modified Krebs–Henseleit buffer 95%O₂ + 5%CO₂ warmed to 37°C). Perfusion fluid was directed into blood vessels and perfused through the entire mass of the organ.

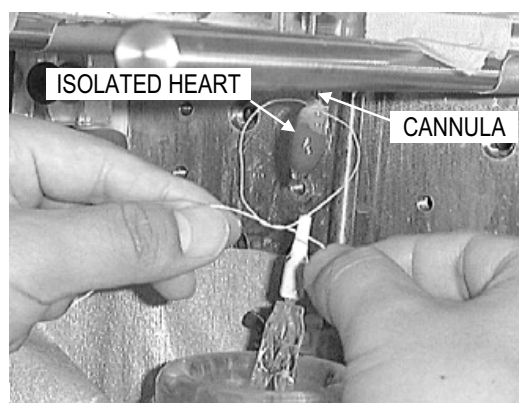


Fig. 4. Isolated perfused rat heart. The aorta was secured to the cannula with a suture.

In the isolated rat heart, contractile function and regular heart rhythm returned within a few seconds. Maximum function was established in several minutes. Arterioles in coronary arteries were visualized by injection of iodine contrast agent into the ascending aorta. The volume of the non-ionic contrast agent used for imaging was 0.4 ml per injection at a rate of 0.2 ml/s. First, baseline angiography was performed; then the contrast agent was washed out from the isolated heart using perfusion with normal perfusate for 10 min. Next, the perfusate was changed to one containing a vasoactive agent; microangiography was performed a second time after 10 min. Microangiography was performed similarly a third and a fourth time with other agents.

Microangiographic images were obtained sequentially at a rate of 30 frame/s and at an X-ray energy of 33.2 keV just above the iodine K-edge energy in the zoom-imaging mode of the detector with the 4.5 mm × 4.5 mm field of view. For the imaging experiment, an X-ray

shutter using a galvanometer-based scanner was used; the exposure time per image was adjusted to 2 ms. Images were stored in the digital-image acquisition system at 10-bit resolution and 1024×1024 -pixel format. During the total imaging time of 1.67 s, 50 frames were acquired. All animal experiments conformed to the SPring-8 Guide for Care and Use of Laboratory Animals.

3.2 Results

The SATICON camera's field of view ($4.5 \text{ mm} \times 4.5 \text{ mm}$) is limited to dimensions smaller than a rat's heart. An angiographic image produced by combining nine separate photographs presented in Fig. 5 was created to show the angiographic anatomy of all vessels in the rat heart: the left anterior descending artery (LAD), the left circumflex coronary artery (LCX), and the right coronary artery (RCA). Angiographic imaging was repeated nine times for the nine imaging regions in a normal rat heart. Each image in Fig. 5 was selected from each angiographic sequence at the same cardiac phase. Consequently, the composite image was formed using nine diastole phase images because the heart ventricles are relaxed and the heart wall motion is slow in the diastole phase.

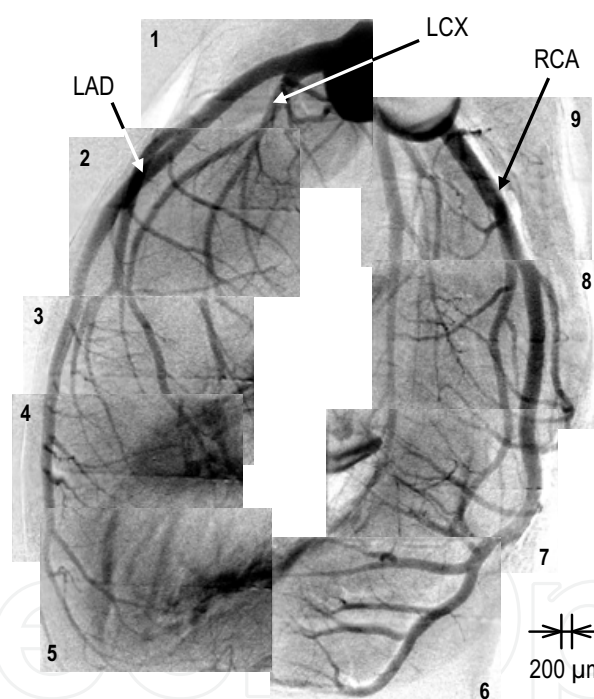


Fig. 5. Composite image of the rat coronary arteries showing the angiographic anatomy of all vessels in a rat heart. The image shows the left anterior descending artery (LAD), the left circumflex coronary artery (LCX), and the right coronary artery (RCA).

The composite whole heart image can exhibit the most suitable region for radiographical evaluation. For this study, the sixth region was selected for evaluation of diameter changes in small coronary arteries. The region includes a few of the right coronary arteries near the cardiac apex. This condition is useful to isolate individual vessels for quantitative analyses of the vessel dimensions.

Figure 6 shows representative coronary artery images of one heart cycle in a normal rat heart corresponding to the sixth region in Fig. 5. The detector's X-ray field of view was $4.5\text{ mm} \times 4.5\text{ mm}$ in the zoom imaging mode, but the images show the area of $4.5\text{ mm} \times 3.2\text{ mm}$ after image trimming. The interval of consecutive images was 33.3 ms; one heart cycle time was 200 ms, corresponding to a heart rate of 300 per minute. Black arrows indicate the direction of the heart wall motion at the diastole and systole phases. The second image in Fig. 6 shows the mid-systole phase in a cardiac cycle. The fourth and fifth images indicate the mid-diastole phase. Compared with the scale bars of $100\text{ }\mu\text{m}$ spacing in the first image, small blood vessels of less than $50\text{ }\mu\text{m}$ diameter were displayed in images. We have succeeded in establishing a new microangiographic technique to visualize rat coronary arteries with high spatial resolution in real time.

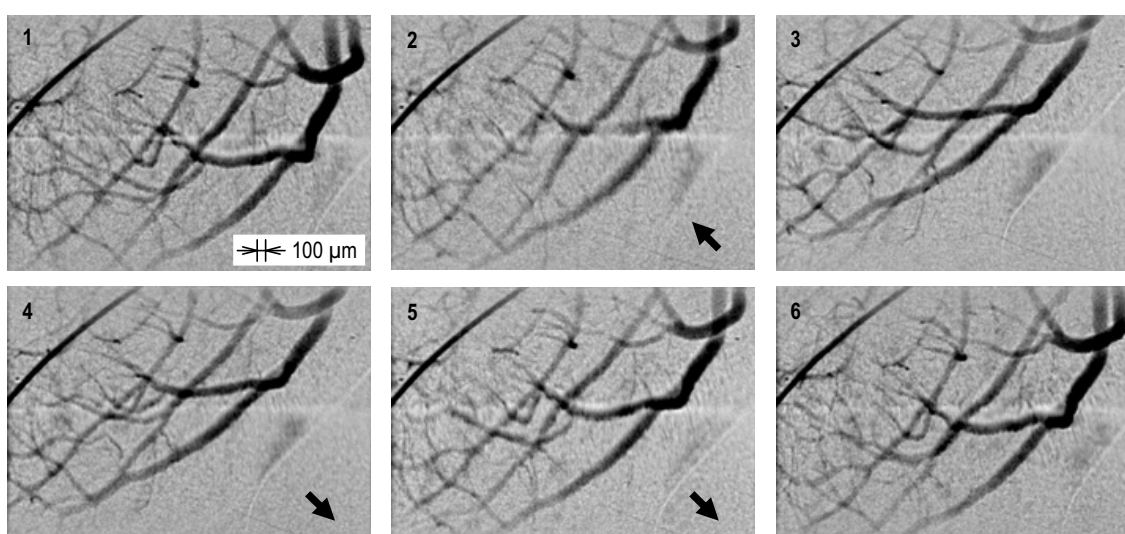


Fig. 6. Sequential images of the right coronary arteries collectively depicting one heart cycle. The interval is 33.3 ms in consecutive images. Black arrows indicate the direction of the heart wall motion.

We directly investigated the effects of hypertension and diabetes on the response of small arteries to drugs. Then, we demonstrated vessel dilation by drug manipulation because the drugs used for this study are known to induce vessel dilation. Figure 7 portrays three sets of right coronary artery images showing the effects of drug manipulation in normal (left column), hypertensive (center column), and diabetic (right column) rat hearts. Each image shows an area of $4.5\text{ mm} \times 4.5\text{ mm}$, which is the same as the detector's field of view. In each column, the first images in the top are the baseline angiogram, the second ones depict responses of coronary arteries under the influence of acetylcholine, the third ones depict the influence of adenosine triphosphate, and the fourth ones depict the influence of sodium nitroprusside. These images portray typical diameter changes or no change of small coronary arteries in response to vasoactive agents. In each column, four pairs of white arrows indicate the same coronary arteries with vessel diameters of less than $200\text{ }\mu\text{m}$.

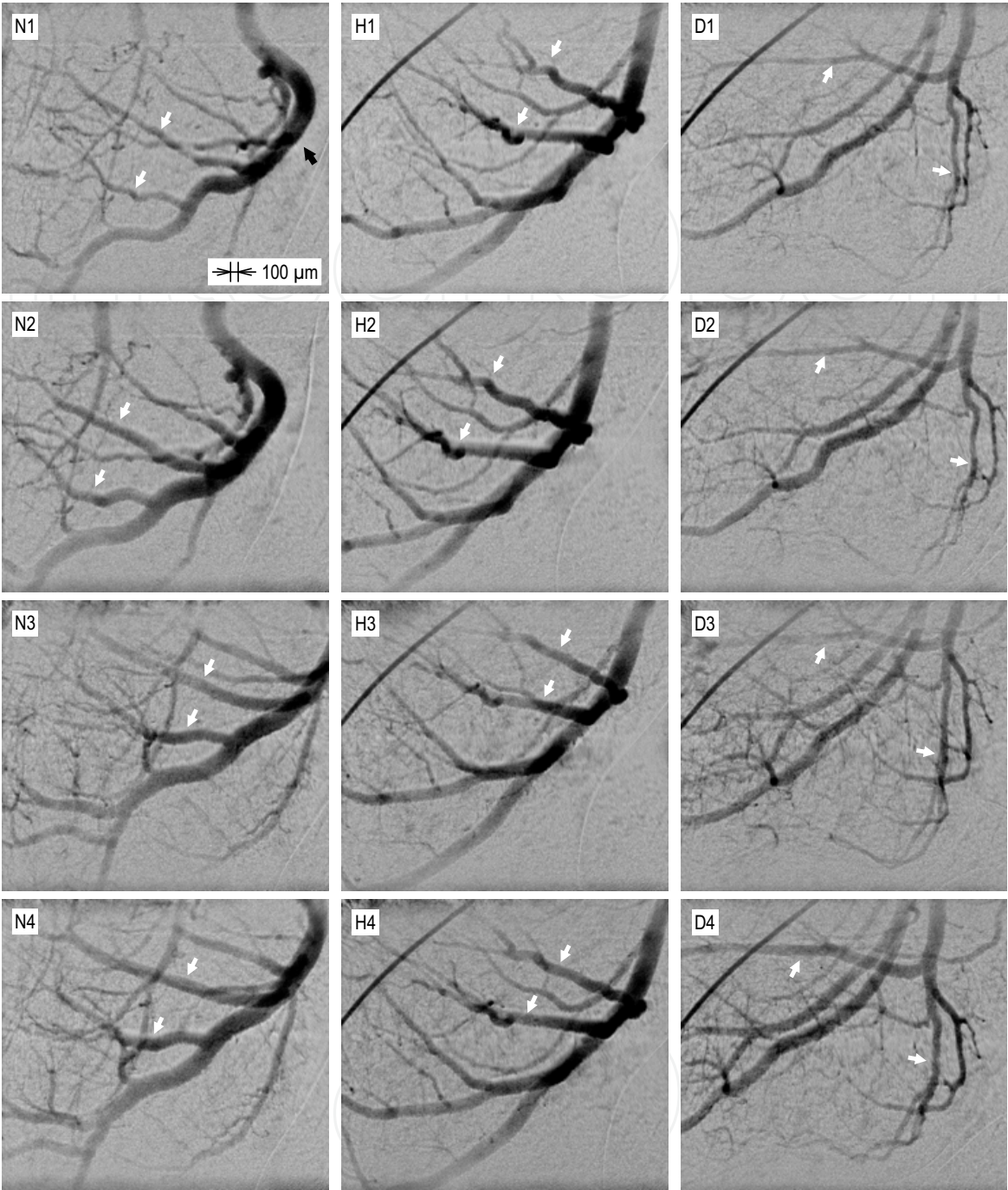


Fig. 7. Three sets of right coronary artery images showing the effects of drug manipulation in normal (N1–N4), hypertensive (H1–H4), and diabetic (D1–D4) rat hearts: (N1, H1 and D1) baseline, (N2, H2 and D2) acetylcholine stress, (N3, H3 and D3) adenosine triphosphate stress, and (N4, H4 and D4) sodium nitroprusside stress.

Small arteries of less than 200 μm diameter are called resistance vessels. The vascular resistance regulates the blood flow by changing the vessel diameter. Only small arteries have a blood flow regulation function. In the normal rat, vasodilatation, indicated by white

arrows in the left column of Fig. 7, was observed in small arteries of less than approximately 200 μm diameter, whereas major trunk vessels (black arrow in Fig. 7(N1)), from which small arteries branch directly, showed almost no change of internal diameter caused by vasoactive agents. The existence of regulation function is determined by the diameter of individual vessels. Third-order branches of coronary arteries are visible in Fig. 7 (N2–N4). Furthermore, new arterial branches are visible in Fig. 7 (N3 and N4). Diameters of these new branches are 20–30 μm . On the other hand, in the hypertensive rat, the four images in Fig. 7 (H1–H4) exhibit no change in vascular caliber (white arrows) over time. Moreover, in the rat with diabetes, the second image in Fig. 7 (D2) shows no change of diameter in acetylcholine stress but the third and fourth images in Fig. 7 (D3 and D4) show vascular response to adenosine triphosphate and sodium nitroprusside stress. New arterial branches with diameters of 20–30 μm are also visible in Fig. 7 (D3 and D4).

4. Discussion

We specifically examined the small arteries (white arrows) that branch off directly from the major trunk (black arrow in N1) in the normal rat image in Fig. 7. Diameters of the arteries (N2–N4) indicated by white arrows were increased by almost two times through dilation compared to the baseline arteries (N1). Furthermore, the apparent increase in the number of small vessels with diameters of less than 50 μm was observed (N3 and N4) because the vasoactive agents might increase the diameter not only of intermediate-size vessels, but also of invisible small blood vessels to visible sizes. Comparison with the scale bars of 100 μm spacing shows that these small arteries have diameters of 20–30 μm . On the other hand, diameters of the arteries larger than 200 μm showed no diameter change. Vessel dilation of the coronary arteries depends greatly on the vascular size. Only small arteries with diameters less than 200 μm have a dilation function. We established a new microangiographic technique to visualize diameter changes and the apparent increase in the number of small vessels in rat coronary arteries with high spatial resolution in real time. The present imaging system enables the direct evaluation of vasodilatation caused by acetylcholine, adenosine triphosphate, and sodium nitroprusside stress.

For the hypertensive rat heart shown in the center column of Fig. 7, no artery exhibited a change of diameter. The images do not display a vascular response to the three vasoactive agents; the results showed that the vasoactive-agent-induced relaxation was considerably impaired. Hypertension can damage the arteries' inner walls. The results reveal the mechanism and effect of disease: vessel dilation of the arteries might be specifically impaired in hypertension. Impairment of vessel dilation function might result in cardiovascular diseases.

For the heart of the rat with diabetes shown in the right column of Fig. 7, the images do not exhibit vascular response to acetylcholine stress but show a response to adenosine triphosphate and sodium nitroprusside stress. However, rates of increase in vessel diameter and in the number of small vessels in dilation compared to the baseline angiogram were smaller than those in the normal rat. We were able to visualize variations in the response among the three vasoactive agents. Acetylcholine-induced relaxation was impaired significantly by dysfunction of the inner walls of arteries, although marked impairment was not observed in adenosine triphosphate and sodium nitroprusside stress. This imaging system can visualize the severity of relaxation impairment directly.

Hypertension and diabetes can cause the inner walls' dysfunction. The synchrotron radiation microangiography system was suitable to investigate characteristics of vascular endothelial function in coronary arteries of rats by taking high-resolution, real-time images. The present system offers the potential of direct investigation into the mechanisms of vascular dysfunctions and is useful to evaluate the severity of damage to arterial inner walls resulting from hypertension and diabetes.

5. Conclusion

Microangiographic imaging with spatial resolution in the micrometer range and at an exposure time of 2 ms was conducted using the combination of the high-speed shutter, the direct-conversion detector, and the nearly parallel X-ray beam provided at SPring-8. Small cardiac blood vessels of less than 50- μm diameter were visualized at heart rates of around 300 per minute in isolated perfused rat hearts. Furthermore, the apparent increase in the number of small vessels with diameters of 20–30 μm was observed after the vasoactive agents increased the diameter not only of intermediate-size vessels, but also that of the invisible small blood vessels to visible sizes. This synchrotron radiation imaging system is a useful tool for depicting large and small coronary arteries in fast-moving hearts and for quantifying actual changes in their diameter caused by vasoactive agents.

Isolated perfused organs provide excellent test-beds for undertaking carefully controlled dose-response studies. Furthermore, these measurements can be made in the absence of confounding effects of other organs. The present imaging system is useful for precise study not only of vascular response, but also of endothelial and smooth muscle function in small blood vessels of less than 50 μm diameter in an isolated perfused heart. Particularly in rat models of metabolic syndrome, the relaxation in response to vasoactive agents can be impaired in coronary arteries compared to normal rats. This angiographic technique will be beneficial for evaluating vascular endothelial dysfunction attributable to metabolic syndrome. Aside from isolated perfused organs, this system offers the potential to investigate mechanisms of vascular dysfunctions directly in any vascular bed (Shirai et al., 2009).

An X-ray imaging system must have a high shutter speed to produce sharp and blur-free images of objects. After the present experiments using the galvanometer-based X-ray shutter system, we developed a rotating-disk X-ray shutter for higher speed imaging. The shutter consists of two disks with radial slots rotating about an axis that is parallel to the X-ray beam. The radial slot width can be changed to adjust the duration of X-ray pulses according to the rotation of one disk with another one. The disks also rotate to match the timing with synchronous signals of the video camera. Using this new shutter system, we have been performing a new line of imaging experiments to investigate the mechanisms of vascular dysfunctions in various vascular beds (Kidoguchi et al., 2006; Morishita et al., 2006; Iwasaki et al., 2007; Shirai et al., 2009).

The authors would like to thank Mr. Tadaaki Hirai and Mr. Toshiaki Kawai of Hamamatsu Photonics K.K. for development of the X-ray SATICON tube. The authors also thank Mr. Sadao Takahashi of Hitachi Denshi Techno-System, Ltd. and Mr. Norio Iwanaga of Zenisu Keisoku Inc. for development of the camera and frame memory system. Synchrotron radiation experiments were performed at the SPring-8 BL28B2 beamline with the approval of the Japan Synchrotron Radiation Research Institute (Acceptance Nos. 2004A0128, 2005A0104, 2006A1493, 2006B1093, and 2007B1052).

6. References

- Colby, L. A. & Morenko, B. J. (2004). Clinical considerations in rodent bioimaging, *Comp Med*, 54, 6, pp. 623–630
- Dix, W. -R.; Kupper, W.; Dill, T.; Hamm, C. W.; Job, H.; Lohmann, M.; Reime, B. & Ventura, R. (2003). Comparison of intravenous coronary angiography using synchrotron radiation with selective coronary angiography, *J Synchrotron Rad*, 10, pp. 219–227
- Grundy, S. M.; Brewer, Jr, H. B.; Cleeman, J. I.; Smith, Jr, S. C. & Lenfant, C. (2004). Definition of metabolic syndrome, *Circulation*, 109, pp. 433–438
- Iwasaki, H.; Fukushima, K.; Kawamoto, A.; Umetani, K.; Oyamada, A.; Hayashi, S.; Matsumoto, T.; Ishikawa, M.; Shibata, T.; Nishimura, H.; Hirai, H.; Mifune, Y.; Horii, M.; Sugimura, K.; Suehiro, S. & Asahara, T. (2007). Synchrotron radiation coronary microangiography for morphometric and physiological evaluation of myocardial neovascularization induced by endothelial progenitor cell transplantation, *Arterioscler Thromb Vasc Biol*, 27, 6, pp. 1326–1333
- Kidoguchi, K.; Tamaki, M.; Mizobe, T.; Koyama, J.; Kondoh, T.; Kohmura, E.; Sakurai, T.; Yokono, K., & Umetani, K. (2006). In vivo X-ray angiography in the mouse brain using synchrotron radiation, *Stroke*, 37, 7, pp. 1856–1861
- Mori, H.; Hyodo, K.; Tanaka, E.; Uddin-Mohammed, M.; Yamakawa, A.; Shinozaki, Y.; Nakazawa, H.; Tanaka, Y.; Sekka, T.; Iwata, Y.; Handa, S.; Umetani, K.; Ueki, H.; Yokoyama, T.; Tanioka, K.; Kubota, M.; Hosaka, H.; Ishikawa, N. & Ando, M. (1996). Small-vessel radiography in situ with monochromatic synchrotron radiation, *Radiology*, 201, pp. 173–177
- Morishita, A.; Kondoh, T.; Sakurai, T.; Ikeda, M.; Bhattacharjee, A. K.; Nakajima, S., Kohmura, E.; Yokono, K. & Umetani, K. (2006). Quantification of distension in rat cerebral perforating arteries, *NeuroReport*, 17, pp. 1549–1553
- Ritman, E. L. (2002). Molecular imaging in small animals—roles for micro-CT, *J Cell Biochem Supp*, 39, pp. 116–124.
- Rubenstein, E.; Hofstadter, R.; Zeman, H. D.; Thompson, A. C.; Otis, J. N.; Brown, G. S.; Giacomini, J. C.; Gordon, H. J.; Kernoff, R. S.; Harrison, D. C. & Thomlinson, W. (1986). Transvenous coronary angiography in human using synchrotron radiation, *Proc Natl Acad Sci USA*, 83, pp. 9724–9728
- Sada, K.; Shirai, M. & Ninomiya, I. (1985), X-ray TV system for measuring microcirculation in small pulmonary vessels, *J Appl Physiol*, 59, pp. 1013–1018
- Shirai, M.; Ikeda, S.; Min, K. -Y.; Shimouchi, A.; Kawaguchi, T. & Ninomiya, I. (1999). Segmental difference in vasodilatation due to basal NO release in in vivo cat pulmonary vessels, *Respir Physiol*, 116, pp. 159–169
- Shirai, M.; Schwenke, D. O.; Eppel, G. A.; Evans, R. G.; Edgley, A. J.; Tsuchimochi, H.; Umetani, K. & Pearson, J. T. (2009). Synchrotron-based angiography for investigation of the regulation of vasomotor function in the microcirculation in vivo, *Clin Exp Pharmacol Physiol*, 36, pp. 107–116
- Service, R. F. (1999). Scanners get a fix on lab animals, *Science*, 286, pp. 2261–2263
- Umetani, K.; Yamashita, T.; Maehara, N.; Tokiya, R.; Imai, S. & Kajihara, Y. (2003). Small-field angiographic imaging of tumor blood vessels in rabbit auricle using X-ray SATICON camera and synchrotron radiation, *Proceedings of 25th Annual International IEEE EMBS Conference*, Cancún, September 17–21, pp. 978–981

- Umetani, K.; Fukushima, K. & Sugimura, K. (2004). Synchrotron radiation microangiography for observation of vasodilatation using X-ray SATICON, *the Journal of the Institute of Image Information and Television Engineers*, 58, 3, pp. 344–351 (in Japanese)
- Umetani, K.; Fukushima, K. & Sugimura, K. (2008). Microangiography system for investigation of metabolic syndrome in rat model using synchrotron radiation, *Proceedings of 30th Annual International IEEE EMBS Conference*, Vancouver, August 20–24, pp. 2693–2696
- Yamashita, T.; Kawashima, S.; Ozaki, M.; Namiki, M.; Shinohara, M.; Inoue, N.; Hirata, K.; Umetani, K. & Yokoyama, M. (2002). In vivo angiographic detection of vascular lesions in apolipoprotein e-knockout mice using a synchrotron radiation microangiography system, *Circ J*, 66, pp. 1057–1059

IntechOpen



Biomedical Engineering

Edited by Carlos Alexandre Barros de Mello

ISBN 978-953-307-013-1

Hard cover, 658 pages

Publisher InTech

Published online 01, October, 2009

Published in print edition October, 2009

Biomedical Engineering can be seen as a mix of Medicine, Engineering and Science. In fact, this is a natural connection, as the most complicated engineering masterpiece is the human body. And it is exactly to help our “body machine” that Biomedical Engineering has its niche. This book brings the state-of-the-art of some of the most important current research related to Biomedical Engineering. I am very honored to be editing such a valuable book, which has contributions of a selected group of researchers describing the best of their work. Through its 36 chapters, the reader will have access to works related to ECG, image processing, sensors, artificial intelligence, and several other exciting fields.

How to reference

In order to correctly reference this scholarly work, feel free to copy and paste the following:

Keiji Umetani, Kazuhito Fukushima and Kazuro Sugimura (2009). Synchrotron Radiation Microangiography for Investigation of Metabolic Syndrome in Rat Model, Biomedical Engineering, Carlos Alexandre Barros de Mello (Ed.), ISBN: 978-953-307-013-1, InTech, Available from: <http://www.intechopen.com/books/biomedical-engineering/synchrotron-radiation-microangiography-for-investigation-of-metabolic-syndrome-in-rat-model>

INTECH
open science | open minds

InTech Europe

University Campus STeP Ri
Slavka Krautzeka 83/A
51000 Rijeka, Croatia
Phone: +385 (51) 770 447
Fax: +385 (51) 686 166
www.intechopen.com

InTech China

Unit 405, Office Block, Hotel Equatorial Shanghai
No.65, Yan An Road (West), Shanghai, 200040, China
中国上海市延安西路65号上海国际贵都大饭店办公楼405单元
Phone: +86-21-62489820
Fax: +86-21-62489821

© 2009 The Author(s). Licensee IntechOpen. This chapter is distributed under the terms of the [Creative Commons Attribution-NonCommercial-ShareAlike-3.0 License](https://creativecommons.org/licenses/by-nc-sa/3.0/), which permits use, distribution and reproduction for non-commercial purposes, provided the original is properly cited and derivative works building on this content are distributed under the same license.

IntechOpen

IntechOpen